Mathematical modeling of cutting effects on flank and bottom edge of end-milling

P.Y. YAPA, A. PALLEGEDARA

pyyehan@gmail.com, achala@eng.pdn.ac.lk

Department of Manufacturing and Industrial Engineering, University of Peradeniya, Sri Lanka

This ongoing study replicates a new mechanistic model for cutting forces in flat-end milling activity. The model considered the total cutting force due to the bottom edge and the flank edge together, which is a unique feature. The model development for flank cutting force coefficients utilizes an exponential function of the instantaneous uncut chip thickness to incorporate size effect for flank cutting in a non-linear least squares algorithm. After the flank cutting force coefficients are calibrated, the instantaneous calibrated coefficients for the bottom cutting force are obtained by calculating the difference between the total measured force and flank force component. This means you can assume the bottom cutting force coefficients are constant values. The cutting force model has been verified through experiments based on different cutting conditions.

Keywords: end-milling, linear least-square method, Levenberg–Marquardt method.

DOI: 10.5604/01.3001.0055.2153

1. Introduction

The end milling machining method finds widespread application across aerospace, automotive, and die-mold industries due to their requirement for high precision and complex shapes. The evaluation of cutting forces stands as a core component of this machining technique because it plays a crucial role in process enhancement through its effects on surface finish, tool durability, and machine stability. Through accurate cutting force modeling manufacturers can improve milling process planning and real-time adaptive control which leads to enhanced productivity while ensuring dimensional precision and extended tool life. The primary difficulty in modeling cutting forces for end milling involves regulating forces along the bottom and flank edges which determines machining efficiency and surface quality while influencing tool longevity and chatter risk. Accurate cutting force modeling becomes necessary when elevated cutting forces cause increased tool wear and vibrations alongside degraded surface quality for process advancement. The findings of this research present a new mechanistic model for cutting forces custom-made for flat-end milling. This model stands out because it assesses the combined cutting forces from both the bottom and flank edge cuts at the same time.

2. Methodology

To account for the size effect while cutting the flanks, the coefficients of the flank cutting force are represented as an exponential function of the current uncut chip thickness and are identified through the non-linear least squares method [6]. With the determined coefficients of the flank cutting force, the bottom cutting force coefficients are real-time adjusted by subtracting the force component of the flank from the total force measurement [6]. While performing a cutting, both the bottom edge as well as the flank of the tool will be in touch with the workpiece. Thus, we have to calculate separately the cutting forces generated from the bottom edge as well as from the flank of the tool, and by summing up, we get the predicted total cutting forces as shown below.

$$F = F_F + F_B \tag{1}$$

3. Calculations of F_F

To determine the cutting force generated by the flank edge, the cutting portion of the cutter along its axis must be segmented into N equal-length disc elements. For the jth disc element within the ith flute of the cutter at φ, the forces acting in the tangential, radial, and axial directions are computed using equations (2) and (3) from [1]. The tangential, axial, and radial forces are then

transformed into *X*, *Y*, and *Z* directions according to Eq. (4) of [1]. The total cutting force exerted on the ith flank edge is derived using Eq. (6) of [1].

4. Calculations of F_B

The force involved in bottom edge cutting can also be characterized by its tangential, radial, and axial components. In fact, bottom edge cutting is essentially the same as the rubbing action described in the dual-force model. Consequently, bottom edge cutting force can be considered directly proportional to the length of the contact line. Based on Equations (7), (8) and (9) from [1], it is possible to calculate the bottom edge cutting force.

5. The determination of instantaneous uncut chip thickness

The parameters $h_{F,i,j}(\varphi)$ and $w_{B,i}(\varphi)$ vary with the angle of cutter rotation and are influenced mainly by run-out of the cutter as per the equations given. The run-out offset ρ denotes the deviation of the cutter's axis from the axis of the tool holder, while λ denotes the angular position at the cutter's lower section measured from the offset direction to
a particular tooth tip. The equation below describes the cutting radius of the associated disc element due to radial run-out influence.

$$R_{i,j}(z) = R + \rho \cos\left[\lambda - \psi(z) - \frac{2(i-1)\pi}{N_f}\right] \quad (2)$$

In this context, $R_{i,j}(z)$ denotes the actual cutting radius associated with the jth cutting disk component of the i-th flank edge at position z, while R indicates the nominal cutter radius. The notation $\psi(z)$ refers to the radial lag angle at position z. Given that each disc element is relatively small, the value of z is considered to be the axial coordinate of the midpoint corresponding to the relevant disc element. As run-out of the cutter occurs, $h_{F,i,j}(\varphi)$ is computed according to Eq. (12) referenced in [1]. In this study, we employed specific methods to ascertain the values of ψ(z). To determine the axial pitch L, we utilized the cutter diameter D alongside the helix angle λ as described below:

$$L = \frac{\pi D}{\tan(\lambda)} \quad (3)$$

D represents the cutter diameter (in m). Then, λ is defined as the helix angle (also converted to radians in the calculation). The vertical distance a tooth moves in one full rotation of the cutter is called axial pitch. The radial lag angle φ(z) on the axial depth z can be calculated using the following equation

$$\psi(z) = \frac{2\pi z}{N_f L} + \phi_{\text{phase}} \quad (4)$$

where z is the axial coordinate (mm). N_f is the number of teeth in the cutter. L is the axial pitch (mm). The phase shift of every tooth is ϕ_{phase}.

The equation identifies how ψ(z) varies along the axial position of a certain cutter tooth. Used the Python-based algorithm for the calculation. We will start by entering the cutter diameter (D), the helix, and the number of teeth (N_f). The angle of the helix is converted into a radian from a degree. After that, the axial pitch (L) has been derived from Eq. (3). To calculate ψ(z) using an equation, it is necessary to set an initial axial depth value $z0$, and a discrete incremental step value Δz (4). After every 10 calculations the axial depth resets to $z0$ in order to show the periodicity of the cutter geometry. The computed values of ψ(z) are then arranged into a table and saved to an Excel file for analysis.

To find the flute that is active during cut operation, the value of indexing parameter $m_{i,j}$ is calculated based on geometry of cutter and processing parameters. To perform this calculation, we require the following inputs: the cutter runout amplitude ρ (mm), nominal cutter radius r (mm), width of cut W (mm), and number of flutes N_f [3]. The maximum indexing value $j_{\max}$ is set to 10, indicating the number of angular divisions. The basic angular step size θ_0 (radians) is defined to control the resolution of this indexing process. These parameters are important for the cutter's flutes interaction with the workpiece and for tracking the flute that removes material at each increment of theta. The engagement angle h in radians is calculated using:

$$h = 2\cos^{-1}\left(1 - \frac{2W}{2r}\right) \quad (5)$$

This formula ensures that the width of cut does not exceed the cutter diameter ($2r$). The phase shift factor ψ_{factor} accounts for cutter runout and is given by:

$$\psi_{\text{factor}} = \frac{\rho}{r \cdot j_{max}} \quad (6)$$

For each flute i (i = 1, 2, 3) and for each indexing value j (j = 1, 2,..., 10), the angular position $\theta_{i,j}$ is calculated as:

$$\theta_{i,j} = \begin{cases} j \cdot \theta_0, & i = 1 \\ \frac{2\pi}{N_f} + j \cdot \theta_0, & i = 2 \\ \frac{4\pi}{N_f} + j \cdot \theta_0, & i = 3 \end{cases} \quad (7)$$

The phase shift ψ_j for each step j is computed as:

$$\psi_j = j \cdot \psi_{\text{factor}} \quad (8)$$

Finally, the indexing parameter $m_{i,j}$ is computed using:

$$m_{i,j} = \left[1 + \left\lfloor \frac{\theta_{i,j} + \psi_j + h}{2\pi/N_f} \right\rfloor\right] \; mod N_f + 1 \quad (9)$$

The floor function is denoted as $\lfloor \cdot \rfloor$, and its function is to ensure that every flute indexing value obtained remains an integer. Also, a modulator operation is used to keep the flute in periodic status. This means that flute index is confined within the range 1 to N_f, where N_f is the total number of flutes on the cutter. This method maintains the same indexing throughout multiple rotations of the cutter. It is important for determining the flute that is engaged at a given angular position. Accurate calculation of the instantaneous uncut chip thickness $h_{F,i,j}(\varphi)$ requires many input parameters. The feed per tooth f (mm), runout amplitude of cutter ρ (mm) and the angle of runout base location λ_{base} (radians).

Also, the number of cutter teeth N_f and the cutter radius R (mm) and angular increment factor θ_{factor} (radians) which both have a nominal value of 3 in the present investigation. Next, the radial lag angle ψ_z (in radians) is also needed at each step of the axial depth. Furthermore, the indexing parameter $m_{i,j}$ defines the flute active in the cut at every angle. When these parameters are combined, they will help in a better and accurate understanding of chip thickness variability during end milling.

For each flute i ($i = 1, 2, 3$), the runout location angle λ_i is computed as:

$$\lambda_i = \lambda_{\text{base}} + \frac{2(i-1)\pi}{N_f} \quad (10)$$

The angular position for the j-th indexing step of the i-th flute is calculated by:

$$\theta_{i,j,\varphi} = j \times \theta_{\text{factor}} \quad (11)$$

The effective cutter radius at the j-th indexing step of the i-th flute, $R_{i,j}$, and the corresponding previous flute position $R_{i-mi,j}$ are given by:

$$R_{i,j} = R + \rho \cos(\lambda_i - \psi_z) \quad (12)$$

$$R_{i-m_{i,j}} = R + \rho \cos\left(\lambda_i - \psi_z - \frac{2\pi \cdot m_{i,j}}{N_f}\right) \quad (13)$$

At each cutting position, the instant uncut chip thickness is given by (12) in [1]. The procedure for finding instantaneous uncut chip thickness is carried through several phases. The runout location angle λ_i is first determined for every flute i. Next, the relevant radial lag angle ψ_z is identified for flute i and indexing step j. After that, we obtain this suitable indexing value $m_{i,j}$ which indicates the active flute at that particular position. The flute geometry and indexing step calculate the angular position $\theta_{i,j,\varphi}$. Using the parameters, effective cutter radii $R_{i,j}$ and $R_{i-mi,j}$ which reflect cutter runout effects are determined. Eventually, the instantaneous uncut chip thickness $h_{F,i,j,\varphi}$ can be determined by applying the governing equation to the relevant geometric and process variables defining chip formation.

6. Calibration of cutter runout parameters

At the beginning of a tooth cycle, all cutting force signals suggest that any tooth can remove the material left by the previous tooth. In this instance, the value of $m_{i,j}$ is given as 1. Also, for the purpose of cutter runout parameters adjustment, the lower cutting force coefficients, $K_{B,q}$ (where $q = T, R, Z$) are taken as constant values. This assumption will be verified in Section 8. Previous studies have shown that the cutting force coefficients and the current uncut chip thicknesses are not linearly correlated. The sharper the cutting force coefficient, the lower the instantaneous uncut chip thickness. The size effect happens when chip thickness is less, but the effect is much less when chip thickness is more. In down milling, if one chooses a high value of feed per tooth, and the radial depth of cut is equal to (or practically equal to) the cutter radius, then the total cutting forces will mainly depend on the flank instantaneous uncut chip thickness. This phenomenon occurs because during the initial moment of the tooth cycle, only the leading disc element of any edge will be cutting. This correlation can be mathematically formulated to derive the Eq. (14) in [1]. The assertion that solely the initial disc element of any edge is involved in the cut during the main phase of each tooth cycle implies that, at any given cutter rotation angle, there can be a maximum of one cutter edge engaged in the cutting process. This statement is valid when the pertinent cutting process parameters meet the following inequality [5]:

$$\cos^{-1}\left(1-\frac{R_r}{R}\right)+\frac{R_z\tan(\beta_0)}{R}\leq\frac{2\pi}{N_f} \quad (14)$$

After the first parameters are set, a systematic way of calculating the cutter runout amplitude ρ and runout location angle λ will follow. The values of axial depth R_z and radial depth R_r are chosen initially, using the criteria given in Eq. (14). In order to keep cutting force coefficients steady, the feed per tooth must be large enough to minimize size effect, while radial depth of cut should be similar to cutter radius. After optimizing these conditions, a cutting test is conducted. Afterwards, the cutting forces $F_s{}^m(\varphi_{i,1})$ are recorded at the instant when only the first disc element of each flank edge completely contacts the workpiece. The measurement sampling interval must equal the elemental lag angle calculated as a way of ensuring that this instant is captured accurately.

$$\Delta\varphi=\frac{R_z\tan(\beta_0)}{NR} \quad (15)$$

Where the superscript m indicates measured data. The measured forces $F_s{}^m(\varphi_{i,1})$ are then used to replace the theoretical forces $F_s(\varphi_{i,1})$ in Eq. (14) from [1]. Along with Eq. (16) in [1], this facilitates the formulation of a linear system of equations with N_f unknowns to determine $h_{F,i,j}(\varphi)$. Utilizing these expressions and the known quantity of $h_{F,i,1}(\varphi)$, a system of equations is created by implementing Eq. (13). This leads to a matrix equation represented as Eq. (17) in [1], which relates the cutting force parameters, runout angle, and chip thickness. To streamline the solution process for this system, trigonometric identities are employed to convert it into a matrix-vector format, similar to Eq. (18) in [1]. The results for ρcos(λ) and ρsin(λ) are derived using the linear least-squares approach, as demonstrated in Eq. (19) in [1]. Finally, the actual values for ρ and λ are established through the following equations:

$$\lambda=\arctan\left(\frac{g_2}{g_1}\right) \quad (16)$$

$$\rho=\frac{g_1}{\cos\lambda} \quad (17)$$

or

$$\rho=\frac{g_2}{\sin\lambda} \quad (18)$$

The correct solution is that value of λ which yields positive ρ in the interval [0,2π]. In addition, to minimize noise signals in solution generation, it is better to utilize force components of larger magnitudes, for example, the $F^m{}_Y(\varphi_{i,1})$ component of Eq. (14) in [1].

7. Calibration of flank cutting force coefficients

It is necessary to identify six parameters in this section that are k_q and m_q, where q is either T or R or Z. To get the coefficients related to flank edge cutting, both k_q and m_q must be obtained separately so that the influence of the bottom edge cutting is excluded. This process separates the flank cutting forces from the overall cutting forces that are measured. When two tests are performed at identical spindle speeds, radial depths of cut, and feeds per tooth, while only varying the axial depths, the cutting forces associated with one flank edge segment of the cutting edge can be derived by taking the difference in forces of the smaller axial depth test from the larger one case. The difference will help to calibrate of the value of k_q and m_q. The method for calibration is explained in detail below.

Using the cutter run-out values given in Point 6, the $h_{F,i,j}(\varphi)$ values can be determined according to Eq. (12) in [1]. Also, the experimental sampling interval coincides with the elemental lag angle as noted in Section 6, which means that condition (20) in [1] can be formed for every sampling point together with the predicted forces. A meticulous view of this system of equation shows that the force in the X and Y direction is independent of Z direction. With this, the parameters k_T, k_R, m_T, and m_R can be determined independently of k_Z and m_Z. The former two parameters are associated with tangential and radial cutting forces, respectively. The method of Levenberg–Marquardt is used as the approximate solution of k_T, k_R, m_T, and m_R, and the detailed procedure is as follows [4].

a. Remove the lines related to Z-forces in Eq. (30) in [1]. Then a simpler equation system was achieved.
b. Find the initial values of the cutting force coefficients for the first iteration step. Using the equation, assuming $m_T = 0$ and $m_R = 0$. As per [1], the following equation system is obtained.

$$EY=F \quad (19)$$

The calculation of matrix E is based on the sum of altered cutting forces. The individual elements of E are defined as follows:

$$E_{n,1,1}=\sum_{k=1}^{n}-\cos(a\theta_1)\,h_{F,i,j,\varphi_k}w \quad (20)$$

$$E_{n,1,2}=\sum_{k=1}^{n}-\sin(a\theta_1)\,h_{F,i,j,\varphi_k}w \quad (21)$$

$$E_{n,2,1}=\sum_{k=1}^{n}sin(a\theta_1)h_{F,i,j,\varphi_k}w \quad (22)$$

$$E_{n,2,2}=\sum_{k=1}^{n}-\cos(a\theta_1)\,h_{F,i,j,\varphi_k}w \quad (23)$$

In this context, $h_{F,i,j,\varphi,k}$ represents the chip thickness at the angular position φ_k, while θ_1 designates the angular increment in radians. The value of the variable, w, which represents the axial length of the disc element, is 0.001 m. The computational sequence is defined by an index a that follows certain rules and starts at 1 and increases to 10. For odd values of n, the index a increments by 1; however, when it reaches 10, it resets back to 1. In contrast, for even values of n, the index a stays the same. These indexing guidelines ensure that the disc elements are properly sequenced across the angular positions throughout the force modeling process. The final representation of E as a column matrix is provided as:

$$\mathbf{E} = \begin{bmatrix} \begin{bmatrix} E_{1,1,1} & E_{1,1,2} \\ E_{1,2,1} & E_{1,2,2} \end{bmatrix} \\ \begin{bmatrix} E_{2,1,1} & E_{2,1,2} \\ E_{2,2,1} & E_{2,2,2} \end{bmatrix} \\ \vdots \\ \begin{bmatrix} E_{30,1,1} & E_{30,1,2} \\ E_{30,2,1} & E_{30,2,2} \end{bmatrix} \end{bmatrix} \quad (24)$$

Every sub-matrix represents the computed transformation matrix for a particular summation index n. The comprehensive matrix E consists of 30 rows that align with each stage in the calculation.

Then, set $x^{(0)} = [k_T \ 0 \ k_R \ 0]^T$ as the starting point of the whole iteration, where k_T and k_R are solved from Eq. (19), using the linear least-square method. Set $k = k + 1$, $\alpha = \alpha_1$, and $x^{(k)} = x^{(k+1)}$. We use α_1 to avoid matrix singularity [1]. Then calculate $f^{(k)}$ and the Jacobian matrix of Eq. (21) in [1]. Then update $f^{(k+1)}$ by substituting $x^{(k+1)}$ into Eq. (24) in [1]. Once $(f^{(k+1)})^T f^{(k+1)} < < (f^{(k)})^T f^{(k)}$ go to step 2. Otherwise, go to step 1.

1. If $\|(J^{(k)})^T f^{(k)}\| < \varepsilon$, stop iteration. Otherwise, set $\alpha = \beta\alpha$ and go to step and update $x^{(k+1)}$. This $\beta (< 1)$ is used to ensure the convergence.
2. If $\|(J^{(k)})^T f^{(k)}\| < \varepsilon$, stop iteration. Otherwise, set $k = k+1$, $\alpha = \alpha_1$, and $x^{(k)} = x^{(k+1)}$.

As the final solution, you will get $k_T^{(k)}$, $m_T^{(k)}$, $k_R^{(k)}$, and $m_R^{(k)}$, k_Z and m_Z can be similarly determined according to this procedure.

8. Calibration of bottom cutting force coefficients

By utilizing the previously identified flank cutting force coefficients and cutter run-out parameters, the anticipated flank cutting forces can be computed using Eqs. (2)–(6) from [1]. At this point, $K_{B,q}$ can be readily adjusted by solving linear equations as

$$K_{B,q} = \frac{F_{B,q}^{mc}(\varphi_{i,j})}{w_{B,i}(\varphi_{i,j})}, \quad (q = T, R, Z) \quad (25)$$

After the coefficient corresponding to every sampling point is obtained, the mathematical relationship between $K_{B,q}$ and the bottom uncut chip width can be obtained by the fitting method.

9. Results and discussions

A set of cutting tests without any cooling was conducted using a vertical machining center with three axes, specifically the lv 85 pinnacle, to validate the proposed cutting force model and the calibration method. A three-fluted flat-end mill with a diameter of 12.7 mm and a helix angle of 30 degrees was utilized. Cutting forces were recorded using a Kistler 9257B dynamometer along with a Kistler 5019A charge amplifier. To acquire data from the system, an NI USB-6002 Multifunction DAQ Data Acquisition Card and NI DAQExpress Software were employed. The workpiece material used in the tests is aluminum alloy 6063. The relevant cutting parameters are provided in Table 1 and were sourced from [6]. In this ongoing study, Test 1 is employed to assess the parameters related to cutter run-out, utilizing the methodology outlined in Section 3.1. Tests 7 and 8 are performed to calibrate the flank and bottom-cutting force coefficients based on the algorithms described in Sections 3.2 and 3.3, following the currently developed Python scripts. Tests 2 and 3 serve for verification purposes. The calibrated values for the ρ and λ cutter runout parameters are found to be 31.49 μm and 5.39°, respectively. The cutting force coefficients are adjusted according to the method proposed in [6]. In the ongoing research involving the current Python code, k_Z and m_Z can be independently computed from k_T, m_T, k_R, and m_R [6]. The initial values for k_T, k_R, and k_Z were 7.57347 N/mm, 1.30883 N/mm, and –1.65229 N/mm, respectively. After applying the Levenberg–Marquardt Method, the coefficient values obtained for k_T, m_T, k_R, m_R, k_Z, and m_Z were 871785.3324 N/mm, 4.4213, –24.7037 N/mm, –0.04484, –285436.9771 N/mm, and 5.0976, respectively. The values derived from the Levenberg–Marquardt Method for $(J^{(k)})^T f^{(k)}$, which include k_T, m_T, k_R, and m_R along with k_Z and m_Z, are illustrated in Figures 1 and 2, respectively. Figures 3, 4, 5, and 6 display the predicted cutting forces from the flank edge, bottom edge, total predicted forces, and

experimental forces for test 2. Similarly, the predicted cutting forces from the flank edge, bottom edge, total predicted forces, and experimental forces for test 3 are represented in Figures 7, 8, 9, and 10, respectively.

The figure for Test 2 shows the expected lateral edge, bottom edge, total expected forces as well as the experimentally measured forces in Figures 3, 4, 5, and 6, respectively. The same can be said for the result belonging to Test 3, which has been displayed in Figure 7 through Figure 10. The prediction model shows a strong correlation concerning flank edge forces, effectively reflecting the expected force behaviors. The middle part of the cut witnessed a surprising uptick in the magnitudes of the bottom-edge cutting forces which seems unreasonable. Research is still focusing on the issue and is being investigated at the present time. Also, the force data found experimentally was quite noisy and variable, such that clear and consistent trends are hard to find. In upcoming experiments, a laboratory-grade amplifier will be used to filter these signals. This will improve the signal characteristics and help further specify force patterns.

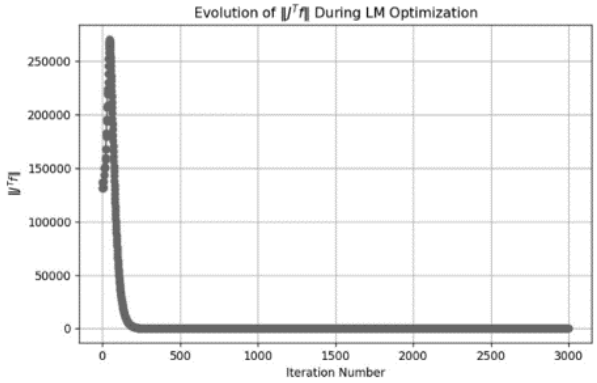

Fig. 1. Levenberg iterations to find k_T, m_T, k_R, and m_R

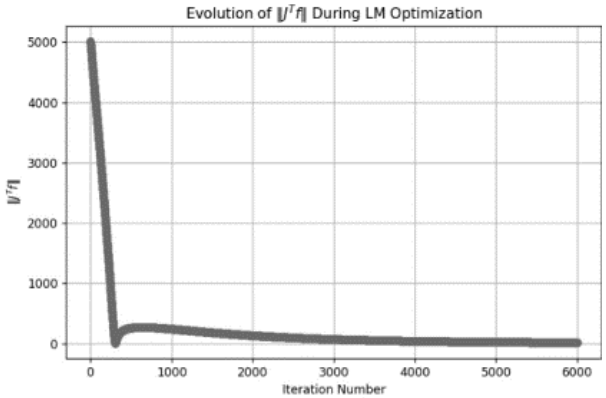

Fig. 2. Levenberg iterations to find k_Z and m_Z

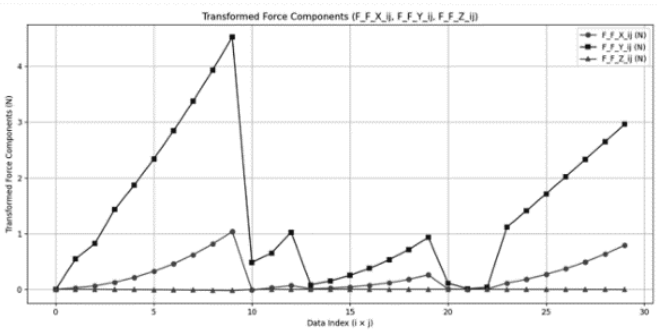

Fig. 3. Predicted Flank cutting forces for test 2

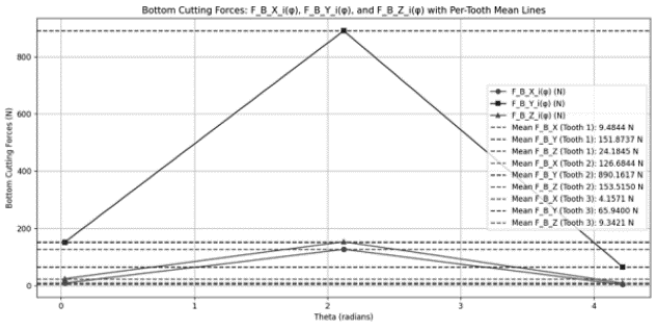

Fig. 4. Predicted Bottom cutting forces for test 2

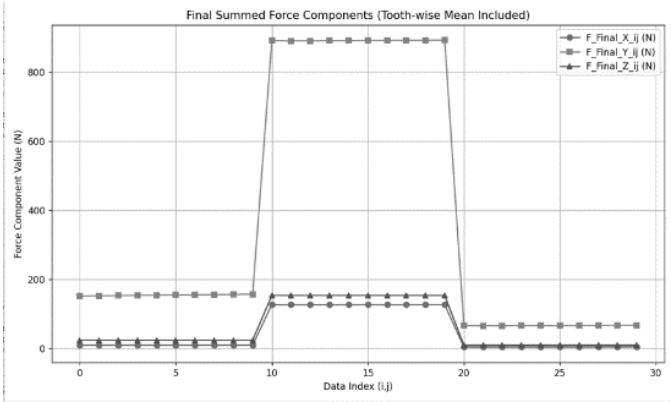

Fig. 5. Predicted total cutting forces for test 2

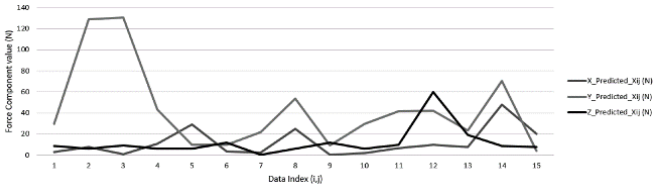

Fig. 6. Experimental forces for test 2

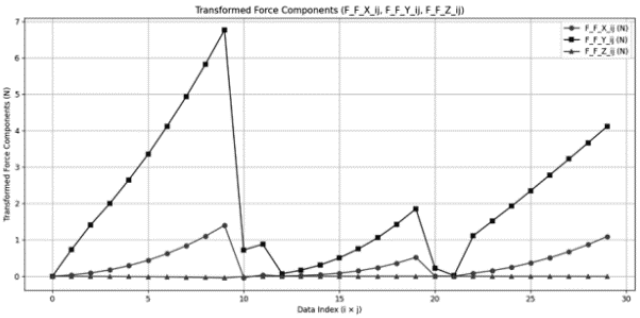

Fig. 7. Predicted Flank cutting forces for test 3

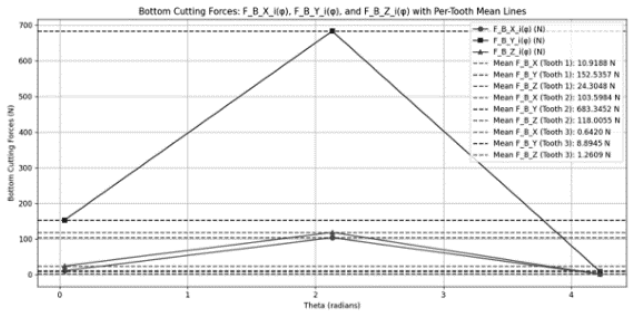

Fig. 8. Predicted Bottom cutting forces for test 3

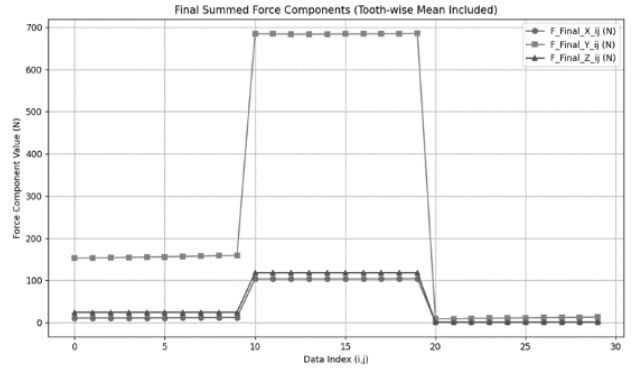

Fig. 9. Predicted total cutting forces for test 3

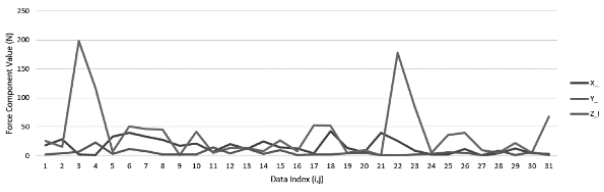

Fig. 10. Experimental cutting forces for test 3

Tab. 1. Cutting Parameters and Cutting Conditions

Test No.	Radial Depth R_r (mm)	Axial Depth R_z (mm)	Feed per Tooth f (mm)	Spindle Speed (rpm)
1.	6	5	0.06	2000
2.	3	3	0.03	2000
3.	3	4	0.03	2000
4.	6	2	0.053	2000
5.	5	3	0.08	1000
6.	2	8	0.033	2000
7.	6	1	0.05	2000
8.	6	10	0.05	2000
9.	6	3	0.06	2000
10.	12	3	0.022	3000
11.	3	4	0.03	6000

10. Acknowledgments

I wish to express my heartfelt gratitude to the Head of the Department of Manufacturing & Industrial Engineering at the University of Peradeniya for providing the equipment and instruments to carry out the experiments and run the simulations. I acknowledge and appreciate the technical officers who assist in carrying out experimental operation and collecting data on machining processes. Finally, I would like to thank every individual involved in helping me conduct this research as this project would have not been possible without any of the above.

11. Bibliography

[1] Wan M., Zhang W.H., Dang J.W., Yang Y., "A novel cutting force modeling method for cylindrical end milling", *Applied Mathematical Modelling*, 34(3), 823–836 (2010).

[2] Shin Y.C., Waters A.J., "A new procedure to determine instantaneous cutting force coefficients for machining force prediction", *International Journal of Machine Tools and Manufacture*, 37(9), 1337–1351 (1997).

[3] Ko J.H., Yun W.-S., Cho D.-W., Ehmann K.F., "Development of a virtual machining system, Part 1: Approximation of the size effect for cutting force prediction", *International Journal of Machine Tools and Manufacture*, 42(15), 1595–1605 (2002).

[4] Wan M., Zhang W.H., Tan G., Qin G.H., "New algorithm for calibration of instantaneous cutting-force coefficients and radial run-out parameters in flat end

milling", *Journal of Engineering Manufacture*, 221(6), 1007–1019 (2007).
[5] Dang J.W., Zhang W.H., Yang Y., Wan M., "Cutting force modeling for flat end milling including bottom edge cutting effect", *International Journal of Machine Tools and Manufacture*, 50(11), 986–997 (2010).
[6] Budak E., Altintas Y., Armarego E.J.A., "Prediction of milling force coefficients from orthogonal cutting data", *Journal of Manufacturing Science and Engineering*, 118(2), 216–224 (1996).

Modelowanie matematyczne efektów skrawania na powierzchni bocznej i dolnej krawędzi frezowania trzpieniowego

P.Y. YAPA, A. PALLEGEDARA

Niniejsze badanie replikuje nowy mechanistyczny model sił skrawania podczas frezowania czołowego. Model uwzględnia całkowitą siłę skrawania pochodzącą od dolnej krawędzi i krawędzi bocznej, co jest unikalną cechą. Opracowanie modelu współczynników siły skrawania bocznego wykorzystuje funkcję wykładniczą chwilowej grubości wióra nieobrobionego, aby uwzględnić wpływ rozmiaru skrawania bocznego w nieliniowym algorytmie najmniejszych kwadratów. Po skalibrowaniu współczynników siły skrawania bocznego chwilowe skalibrowane współczynniki siły skrawania dolnego są uzyskiwane przez obliczenie różnicy między całkowitą zmierzoną siłą a składową siły bocznej. Oznacza to, że można założyć, że współczynniki siły skrawania dolnego są wartościami stałymi. Model siły skrawania został zweryfikowany eksperymentalnie w różnych warunkach skrawania.

Słowa kluczowe: frezowanie czołowe, metoda najmniejszych kwadratów liniowych, metoda Levenberga–Marquardta.